AIChE

Cycle Synthesis and Optimization of a VSA Process for Postcombustion CO_2 Capture

Reza Haghpanah, Ricky Nilam, and Arvind Rajendran
School of Chemical and Biomedical Engineering, Nanyang Technological University, 62 Nanyang Drive, Singapore 637459

Shamsuzzaman Farooq and Iftekhar A. Karimi
Dept. of Chemical and Biomolecular Engineering, National University of Singapore, 4 Engineering Drive, Singapore 117576

DOI 10.1002/aic.14192
Published online August 23, 2013 in Wiley Online Library (wileyonlinelibrary.com)

A systematic analysis of several vacuum swing adsorption (VSA) cycles with Zeochem zeolite 13X as the adsorbent to capture CO_2 from dry, flue gas containing 15% CO_2 in N_2 is reported. Full optimization of the analyzed VSA cycles using genetic algorithm has been performed to obtain purity-recovery and energy-productivity Pareto fronts. These cycles are assessed for their ability to produce high-purity CO_2 at high recovery. Configurations satisfying 90% purity-recovery constraints are ranked according to their energy-productivity Pareto fronts. It is shown that a 4-step VSA cycle with light product pressurization gives the minimum energy penalty of 131 kWh/tonne CO_2 captured at a productivity of 0.57 mol CO_2/m^3 adsorbent/s. The minimum energy consumption required to achieve 95 and 97% purities, both at 90% recoveries, are 154 and 186 kWh/tonne CO_2 captured, respectively. For the proposed cycle, it is shown that significant increase in productivity can be achieved with a marginal increase in energy consumption. *AIChE J*, 59: 4735–4748, 2013
Keywords: carbon capture, dynamic simulation, genetic algorithm, optimization, vacuum swing adsorption

Introduction

The importance of mitigating anthropogenic climate change has been intensely pursued since the later part of the last century, leading to the formation of the Intergovernmental Panel on Climate Change by the United Nations. There is now a general consensus that the emission of greenhouse gases, which is predominantly CO_2 from the combustion of fossil fuel, contributes to global warming.[1] Despite that, the energy sectors worldwide are still overwhelmingly dependent on fossil fuels to meet about 85% of the global energy demand.[2] In the absence of economically viable renewable energy sources at present, and with the abundance of low-cost fuel such as coal, it is likely that fossil fuels will continue to be the dominant source of energy for decades to come. Thus, technologies that allow the continued use of fossil fuel while reducing the amount of CO_2 released into the atmosphere are urgently needed.

To mitigate the release of CO_2 into the atmosphere, it has to be captured from emission sources. The captured CO_2 then can be stored in the ocean or underground, or utilized for enhanced oil recovery or enhanced coal bed methane recovery. There are four main approaches to separate CO_2 from flue gas, namely, absorption (chemical or physical), adsorption, membranes, and cryogenic processes.[3] Among these, absorption is the most mature technique and the bulk of CO_2 separation is performed using this process. However, regeneration of solvents in absorption is energy intensive thereby contributing to a high cost of capture.[3,4] With the emergence of various adsorbent materials, adsorption-based separation processes for CO_2 capture are receiving increasing attention as a potential low-energy option.[5,6] There are two main modes of adsorption process: pressure swing adsorption (PSA)[7] and thermal swing adsorption (TSA).[8] Between these two modes, PSA enjoys faster regeneration over TSA. Membrane separation is another promising technology that has gained attention for separation of CO_2 in recent years.[4,9] This process is attractive for CO_2 separation due to its favorable permeation over the other components in the emissions.[3] Cryogenic distillation is energy intensive and heavily relies on the removal of water and many trace components prior to cooling.

A PSA process with operations at both above atmospheric and vacuum pressures is called a pressure-vacuum swing adsorption (PVSA) cycle. Vacuum swing adsorption (VSA) refers to cycling between atmospheric and vacuum pressures. A variety of PVSA/VSA cycles have been developed for the capture and concentration of CO_2 from flue gas. To design an appropriate cycle, it is essential to understand the nature of the separation problem. A typical flue gas from a

Dedicated to Prof. Douglas M. Ruthven on the occasion of his 75th birthday.
Additional Supporting Information may be found in the online version of this article.

Correspondence concerning this article should be addressed to A. Rajendran at this current address: Dept. of Chemical and Materials Engineering, University of Alberta, 9107-116 Street, Edmonton, Alberta, Canada T6G 2V4; e-mail: arvind.rajendran@ualberta.ca or S. Farooq at chesf@nus.edu.sg.

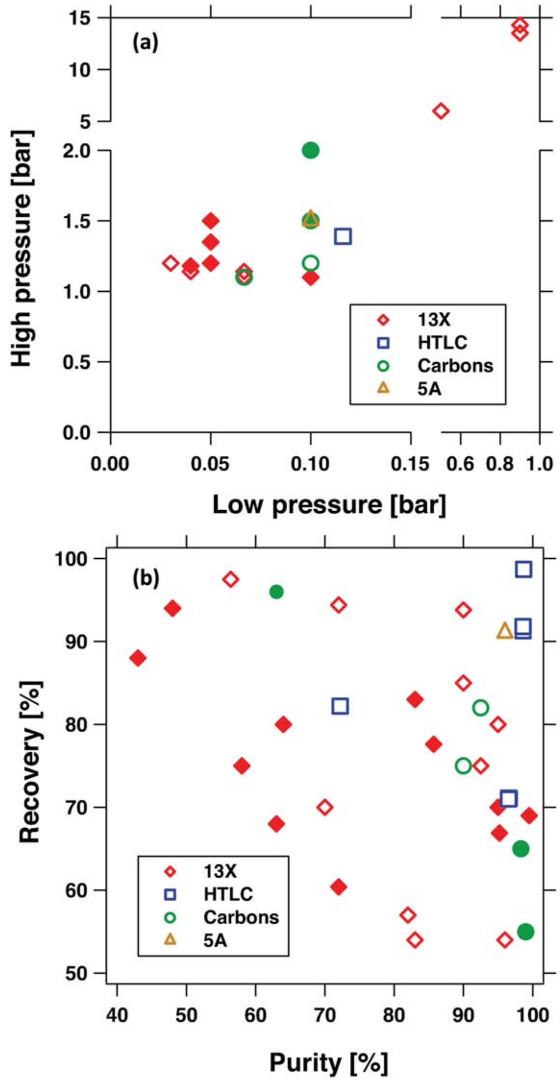

Figure 1. Summary of adsorptive CO_2 capture processes from the literature.

(a) High-pressure and low-pressure levels in different PVSA/VSA cycles reported in the literature for postcombustion CO_2 capture. (b) CO_2 purity/recovery performance. The open and closed symbols represent simulation and experimental studies, respectively. [Color figure can be viewed in the online issue, which is available at wileyonlinelibrary.com.]

postcombustion power plant is at 25–50°C, 1 bar, and consists of ≈15% CO_2 in a predominantly N_2 mixture. While the recovery target set by various regulatory bodies (such as US Department of Energy, DOE) for CO_2 capture and concentration is 90%,[10] the purity targets depend on the type of applications. Typically, CO_2 purities in excess of 90% are expected from these processes. Considering the low concentration of CO_2 in the flue gas, it is important to realize that pressurizing the entire flue gas stream can be expensive. Figure 1a shows the high-and low-pressure levels of different PSA cycles with various adsorbents. It can be seen from this figure that in all studies, the low pressure was below atmospheric and most studies considered 1.1–1.5 bar or nearly atmospheric pressures as the highest pressure, although significantly higher pressures have also been used. The small increase in feed pressure above atmospheric pressure is primarily to overcome the frictional pressure drop in the column, and such cycles are categorized here as VSA cycles. The performances of these cycles are listed in the Supporting Information[5,6,11–27] and the values of CO_2 purity and recovery are shown in Figure 1b. Some of the best cycles with the highest CO_2 purity are discussed below.

Zhang et al. performed VSA experiments using a 3-bed, 9-step cycle, cycling between 1 and 0.05 bar incorporating heavy reflux (HR) and light-end pressure equalization (PE) steps. Further, they also reported results from a 3-bed, 6-step cycle without HR and with two light-end PE steps. For both configurations, they used zeolite 13X and dry flue gas with 12% CO_2 and 88% N_2.[14] CO_2 purity and recovery of 83% was achieved and a power consumption of 124 kWh/tonne CO_2 captured was reported from the 3-bed, 6-step cycle without HR. For the 3-bed, 9-step cycle with HR a purity of 95% and a recovery of 70% was achieved. In another study, they reported the experimental study of a 3-bed, 6-step cycle with a HR step.[13] For this cycle, they achieved 95.2% purity and 66.9% recovery with a power consumption of 290.4 kWh/tonne CO_2 captured. Xiao et al. simulated a 3-bed, 9-step cycle with two PE steps with an evacuation pressure of 0.03 bar. For this configuration, a purity of 92.5% and recovery of 75% with power consumption of 152 kWh/tonne CO_2 captured were reported.[5] Agarwal et al. proposed 2-bed, 6-step and 2-bed, 8-step cycles with light and heavy refluxes (dual reflux) using zeolite 13X.[6] They optimized the 2-bed, 6-step cycle to maximize CO_2 recovery using a superstructure-based approach. The optimum cycle resulted in a CO_2 purity of 95% and a recovery of 80% with a power consumption of 637 kWh/tonne CO_2 captured. They restricted the evacuation pressure to 0.5 bar, which resulted in pressurizing the flue gas up to 6 bar. The 2-bed, 8-step cycle gave the minimum power consumption of 465 kWh/tonne CO_2 captured at 90% purity and 85% recovery.

Reynolds et al. have studied complex cycles involving HR step using K-promoted Hydrotalcite (HTlc) as the adsorbent for CO_2 capture from flue gas containing 15% CO_2, 75% N_2, and 10% H_2O.[12] They considered a stripping VSA that consisted of the following steps: high-pressure adsorption (F), cocurrent purge with heavy product as HR, reverse blowdown or countercurrent depressurization (CnD) from high pressure (P_H) to vacuum pressure (P_L), countercurrent low-pressure purge with light product as light reflux (LR), and light product pressurization (LPP) from P_L to P_H. The best performance was from a 5-bed, 5-step cycle with LR and HR resulting in CO_2 purity and recovery of 98.7%. However, the feed throughput for this cycle was low. Recently, Liu et al.[27] simulated a two-stage VSA process using 5A zeolite for CO_2 capture from a dry flue gas with 15% CO_2 and 85% N_2. They considered a 3-bed, 5-step cycle with HR and LR steps for the first stage and 2-bed, 6-step with LR and PE steps for the second stage. A CO_2 purity of 96% and a recovery of 91% with power consumption of 179.4 kWh/tonne CO_2 captured and productivity of 0.1 mol CO_2/m^3 adsorbent/s were obtained.

Several challenges exist in designing an adsorption-based process for CO_2 capture. First, the high CO_2 purity and recovery (both $\geq$ 90%) required from a feed with low concentration of CO_2 makes the capture process challenging. Second, in all existing adsorbents, CO_2 adsorbs more strongly than N_2 owing to its higher polarity. Thus, enriched CO_2 is recovered as the extract product. Designing PSA cycles for extract purification has not received much attention in the literature as most cycles focus on purifying the raffinate. Third, the flue gas emissions from existing power plants are significantly larger than what existing gas separation plants can handle. For example, a 500 MW postcombustion coal-fired power plant produces approximately 10,000 tonne CO_2 per day, which makes CO_2 productivity and equipment size (such as columns, vacuum pumps, and compressors) critical factors. To increase the CO_2 productivity and reduce plant size, shorter cycle times are needed. Finally, the presence of moisture poses a significant challenge as most commercial adsorbents with high selectivity of CO_2 over N_2 also adsorb water strongly. This reduces the effective adsorbent capacity of CO_2 and lowers process performance.

To evaluate the true potential of PVSA/VSA processes for CO_2 capture with different adsorbents, rigorous cycle synthesis, and optimization are required. In this work, we focus on determining the optimal operating conditions for VSA processes for cost effective separation of CO_2. Despite considerable growth in the practical applications of cyclic adsorption processes, the design and optimization of these processes are still predominantly done by experimental techniques[28] or parametric studies[11–13] It is important to note that by performing a parametric study, it is not possible to arrive at the optimal condition of all process parameters that will maximize/minimize the desired objective(s) while fully meeting the design and operational constraints. The challenge in simulation and optimization of VSA processes lies in the cyclic nature of its operation. The cyclic operation goes through transient states and the process ultimately reaches a cyclic steady state (CSS) in which the state variables at the beginning of each cycle match with those at the end of the cycle. The governing equations describing such processes are a system of coupled partial differential and algebraic equations which often involve sharp fronts moving in space. The nonlinearities and ill-conditioned matrices due to multiple adsorbent layers, nonisothermal effects, and stringent product specifications may lead to the failure of numerical solvers.[29] In addition, the transient operation yields dense constrained Jacobians, which pose heavy computational burden on gradient-based optimization techniques.[29]

The optimization studies available in the literature mostly consider single objective, for example, minimizing energy consumption, maximizing productivity, and so forth.[6,30–34] However, in most real-life industrial processes, the design problem of a PSA/VSA process involves simultaneous achievement of multiple objectives, for example, maximization of productivity and minimization of energy consumption. Often, these objectives are conflicting and cannot be accommodated meaningfully in a single function. Thus, a true multiobjective optimization showing the trade-off among the objectives would be very valuable to engineers for design and operation purposes. Despite its usefulness, multiobjective optimization of PSA/VSA processes has not received much attention in the literature. Ko et al.[35] presented the modified form of the summation of a weighted objective function method for multiobjective optimization of TSA and rapid PSA processes. This method is based on the idea of forming a single objective function by convex combination of the original objectives and solving a series of single objective optimization problems. Sankararao and Gupta[36] applied multiobjective optimization for PSA air separation using simulated annealing with a jumping gene (MOSA-aJG) algorithm for stochastic search of the decision variables. Recently, Fiandaca et al.[37] reported multiobjective optimization using genetic algorithm (GA), also for PSA air separation, where the objectives were to maximize the purity and recovery of N_2. GA has also been used for optimizing variety of other processes[38,39] including chromatography.[40] The main goal of this study is to synthesize a VSA cycle that yields 90% purity and recovery with lower energy consumption than a basic 4-step cycle, which was optimized in our previous publication,[41] by neither going to deep vacuum ($P_L = 0.02$ bar) nor pressurizing the flue gas. We systematically analyze a variety of VSA cycles with Zeochem zeolite 13X as the adsorbent to capture CO_2 from dry, postcombustion flue gas containing 15% CO_2 in N_2. We achieve full multiobjective purity-recovery and energy-productivity Pareto fronts of the analyzed VSA cycles using GA without compromising the rigor of the simulation model.

Modeling of the Adsorption Process

In this article, the adsorption column dynamics are described by a set of partial differential equations. The fluid-phase component balance assumes that the gas is ideal and is at local thermal equilibrium with the solid. The overall gas-phase balance is written to account for the variation of velocity owing to bulk adsorption. The energy balance considers both convective and dispersive transfer of heat along the axial direction and across the column wall. The transport across the wall is described by taking into account both the inside (h_{in}) and outside (h_{out}) heat-transfer coefficients. The adsorbent chosen in this study is zeolite 13X due to its ability to provide high selectivity for CO_2. The equilibrium data for CO_2 and N_2 are measured in our laboratory[42] and a dual-site Langmuir model is fitted to the data

$$q_i^* = \frac{q_{sb,i} b_i c_i}{1 + \sum_{i=1}^{n_{\mathrm{comp}}} b_i c_i} + \frac{q_{sd,i} d_i c_i}{1 + \sum_{i=1}^{n_{\mathrm{comp}}} d_i c_i} \tag{1}$$

where $q_{sb,i}$ and $q_{sd,i}$ are the solid-phase saturation loadings of sites one and two, respectively. The parameters b_i and d_i follow Arrhenius type temperature dependence

$$b_i = b_{0,i} e^{-\frac{\Delta U_{b,i}}{RT}} \tag{2}$$

$$d_i = d_{0,i} e^{-\frac{\Delta U_{d,i}}{RT}} \tag{3}$$

The corresponding isotherm parameters are given in Table 1. The mass-transfer rate is described by the linear driving force model, and the transport mechanism is assumed to be controlled by molecular diffusion in the macropores. The pressure drop along the column is described by the classical Darcy equation. The use of the Ergun equation, although accurate in the description of the pressure drop, was found to have a minor effect on the energy consumption values calculated. The model equations utilized in this study are the same as those in Haghpanah et al., (see Ref 41), a summary of which is made available in the Supporting Information. The equations used for the calculation of energy consumption are based on the assumption of isentropic compression with an inherent efficiency of 72%. The transport parameters, viscosity, heat capacities are considered to be invariant over the entire operating range. The solution of these equations requires suitable initial and boundary

Table 1. Isotherm Parameters for CO_2/N_2 on Zeochem Zeolite 13X

Parameter	CO_2	N_2
b_0 [$m^3\ mol^{-1}$]	8.65×10^{-7}	2.50×10^{-6}
d_0 [$m^3\ mol^{-1}$]	2.63×10^{-8}	0.00
$\Delta U_{b,i}$ [$J\ mol^{-1}$]	-36641.21	-1.58×10^{4}
$\Delta U_{d,i}$ [$J\ mol^{-1}$]	-35690.66	0.00
$q_{sb,i}$ [$mmol\ g^{-1}$]	3.09	5.84
$q_{sd,i}$ [$mmol\ g^{-1}$]	2.54	0.00

conditions. For all of the VSA cycles simulated in this study, the bed is assumed to be initially saturated with pure N_2 at 1 bar and 25°C. Subsequently, the final conditions of a step constitute the initial conditions for the next. The parameters used in the VSA simulations are listed in Table 2. As discussed in our previous publication,[41] we use a finite volume technique to solve the system of highly nonlinear partial differential equations (PDEs). The PDEs are nondimensionalized and discretized into 30 volume elements and the resulting ordinary differential equations are solved using stiff solvers available in MATLAB, such as ode23s.[41] All performance indicators, for example, purity, recovery, productivity, and energy consumption are calculated once the system reaches CSS. A mass-balance error of less than 0.5% for five consecutive cycles is specified as the criterion for attainment of CSS. The number of cycles required to reach CSS varies between 80 and 480 cycles. It is important to note that in all simulations, only one bed is used. In an industrial multibed process, all beds undergo identical sequence of steps. Hence, for cycles constituting uncoupled steps, simulating one bed is adequate to fully capture the performance of a multibed process. For cycles involving steps where two or more beds are coupled, that is, output from one bed is the input for another; output stream data from the source bed are stored in buffers and used for feeding these streams to the receiving bed via linear interpolation. As short time intervals are used for data collection, linear interpolation is found to provide sufficient accuracy.

Optimization Framework

As mentioned earlier, many studies consider CO_2 capture as a single objective problem. However, statutory regulations impose constraints on the purity and recovery of CO_2 and a capture plant should satisfy two objectives of low-parasitic energy consumption and a small footprint, which have direct implications on operating and fixed costs, respectively. As these two objectives are conflicting, it is desirable to understand the trade-off between them by means of a Pareto curve. Our choice of GA as an optimization algorithm is driven mainly by the fact that we use a full model (i.e., no model reduction) of the VSA process based on spatial discretization and temporal integration. This allows us to keep sight of the underlying physics that governs relative improvement from cycle to cycle in our cycle synthesis study. In this way, in addition to addressing CO_2 capture, we also develop a broader understanding of the operating issues associated with heavy-component concentration and recovery in general. Other advantages of GA include its simplicity of implementation, likelihood of getting globally best solutions, and prospect of exploiting parallel computing for speed-up.We use the nondominated sorting genetic algorithm II proposed by Deb et al.,[43] available in the MATLAB global optimization toolbox, for the multiobjective optimization. Furthermore, we utilize the parallelization toolbox in MATLAB for fast processing. All computations reported were carried out on a desktop workstation with two quad-core INTEL Xeon 3.66 GHz processors and 48.0 GB RAM.

In this work, we use a two-stage optimization procedure. First, we consider maximizing purity and recovery to identify cycles that satisfy minimum 90% purity and recovery of CO_2. For the identified cycles, we then consider the minimization of energy and maximization of productivity with CO_2 purity and recovery $\geq 90\%$ as constraints. We define purity and recovery as follows

$$\text{Purity, } Pu = \frac{\text{Total moles of } CO_2 \text{ in extract product (s)}}{\text{Total moles of } CO_2 + N_2 \text{ in extract product (s)}} \tag{4}$$

$$\text{Recovery, } Re = \frac{\text{Total moles of } CO_2 \text{ in extract product (s)}}{\text{Total moles of } CO_2 \text{ fed in to the cycle}} \tag{5}$$

The total number of moles of CO_2 in the above equations are calculated at CSS. The extract product and feed streams that have been used to calculate the performance indicators are shown in the schematic of the synthesized cycles by P and F, respectively. For the second stage, the two objectives are defined as follows

$$\text{Total Energy}, E = \text{Energy required to compress/evacuate } CO_2 + N_2 \tag{6}$$

Table 2. Parameters Used in VSA Simulations

Parameter	Value
Column Properties	
Column length, L [m]	1
Inner column radius, r_{in} [m]	0.1445
Outer column radius, r_{out} [m]	0.1620
Column void fraction, ε [−]	0.37
Particle voidage, ε_p [−]	0.35
Particle radius, r_p[m]	7.5×10^{-4}
Tortuosity, τ' [−]	3
Properties and Constants	
Flue gas pressure, P_f [bar]	1
Feed temperature, T_{feed} [K]	298.15
Ambient temperature, T_a [K]	298.15
Adsorbent density, ρ_s [$kg\ m^{-3}$]	1130
Column wall density, ρ_w [$kg\ m^{-3}$]	7800
Specific heat capacity of gas phase, C_{pg} [$J\ mol^{-1}\ K^{-1}$]	30.7
Specific heat capacity of adsorbed phase, C_{pa} [$J\ mol^{-1}\ K^{-1}$]	30.7
Specific heat capacity of adsorbent, C_{ps} [$J\ kg^{-1}\ K^{-1}$]	1070
Specific heat capacity of column wall, C_{pw} [$J\ kg^{-1}\ K^{-1}$]	502
Fluid viscosity, μ [$kg\ m^{-1}\ s^{-1}$]	1.72×10^{-5}
Molecular diffusivity, D_m [$m^2\ s^{-1}$]	1.30×10^{-5}
Adiabatic constant, γ	1.4
Effective gas thermal conductivity, K_z [$J\ m^{-1}\ K^{-1}\ s^{-1}$]	0.09
Thermal conductivity of column wall, K_w [$J\ m^{-1}\ K^{-1}\ s^{-1}$]	16
Inside heat transfer coefficient, h_{in} [$J\ m^{-2}\ K^{-1}\ s^{-1}$]	8.6
Outside heat transfer coefficient, h_{out} [$J\ m^{-2}\ K^{-1}\ s^{-1}$]	2.5
Universal gas constant, R [$m^3\ Pa\ mol^{-1}\ K^{-1}$]	8.314
Compression/evacuation efficiency, η	0.72

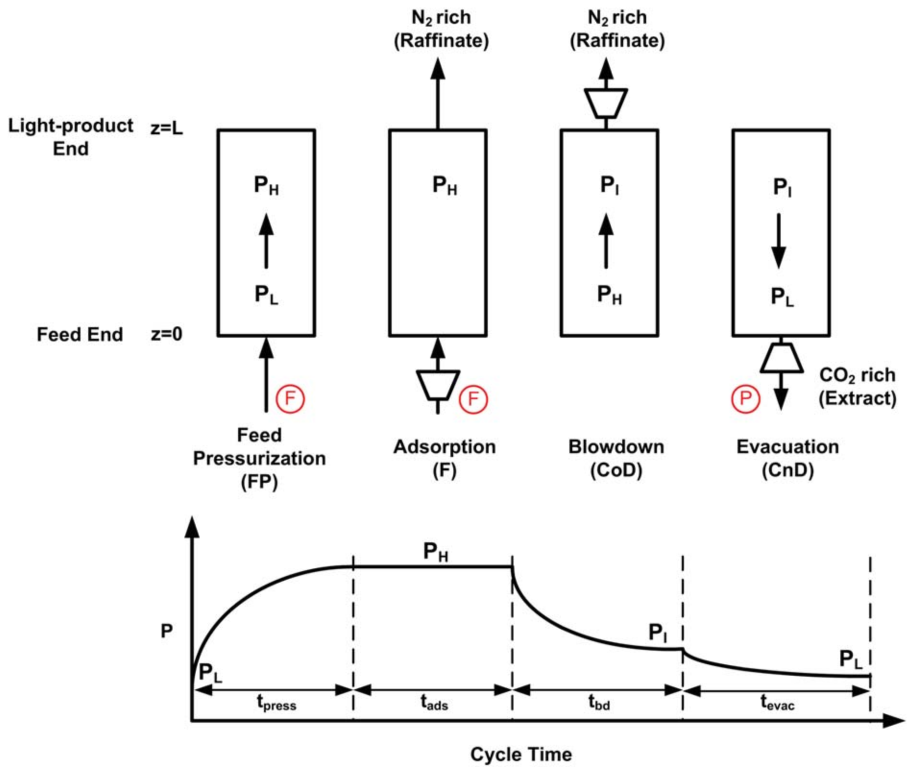

Figure 2. Basic 4-step VSA cycle.

Notations commonly used in the literature are provided within brackets. [Color figure can be viewed in the online issue, which is available at wileyonlinelibrary.com.]

$$\text{Productivity , Pr}=\frac{\text{Total moles of CO}_2\text{in extract product (s)}}{\text{(Total volume of the adsorbent)}\times\text{(Cycle time)}} \tag{7}$$

The energy consumption arises from the vacuum pumps and compressors that are shown in the process schematics. In the case of vacuum pumps, the delivery pressure is assumed to be 1 bar. As the information about purity and recovery are only available after solving the governing PDEs, the purity-recovery constraints are incorporated into the objective functions as penalties. We use 60 generations and 10 times the number of decision variables as the population size.

Maximization of Purity and Recovery

The expected targets for a promising CO_2 capture process are 90–95% purity and 90% recovery of CO_2. Obtaining the complete Pareto front of purity and recovery provides information about the operational flexibility of the process and helps to assess its potential for use in a hybrid configuration, such as adsorption-membrane combination.

To keep the process as simple as possible, we begin with a 4-step cycle described in Figure 2. The process consists of the following steps:

1. Feed pressurization (press, also denoted by "FP" in the literature): Pressurization from the feed end ($z=0$) with fresh feed while the other end ($z=L$) remains closed. The feed is assumed to be at 1 bar and 25°C. The duration of this step is t_{press}. During this step, the column pressure increases from a low (P_L) to feed pressure (P_H).
2. Adsorption (ads, also denoted by "F" in the literature) at feed pressure (P_H): In this step, the light-product end at $z=L$ is open and at 1 bar, and the inlet pressure is calculated using Darcy's equation. The energy required by a blower to increase the pressure of the feed from 1 bar to the inlet pressure is included in the energy consumption. The inlet velocity, v_{feed}, and the duration of the step, t_{ads}, are decision variables.
3. Forward blowdown or cocurrent depressurization (bd, also denoted by "CoD" in the literature): The bed is depressurized to an intermediate pressure (P_I) through the light-product end while the feed end is closed. It is called forward blowdown because the gas flows in the same direction as the feed. The main aim of this step is to remove as much N_2 as possible but retain the CO_2 in the bed. Both intermediate pressure (P_I) and step duration (t_{bd}) are considered as decision variables.
4. Countercurrent evacuation or countercurrent depressurization (evac, also denoted by "CnD" in the literature): The column is evacuated from the feed end to a low-operating pressure (P_L) with the other end closed so that the high-purity extract CO_2 product is obtained, and the adsorbent bed is regenerated. The pressure level (P_L) and step duration (t_{evac}) are used as decision variables.

It was shown in our pervious study (see Ref 41; results reproduced in Figure 3 for convenience) that for the basic 4-step cycle (Figure 2), it is possible to obtain both purity and recovery greater than 90% only with an evacuation pressure close to 0.02 bar or lower. However, this is often difficult to achieve in an industrial column. It is also clear that with P_L=0.03 bar, considered as an industrially achievable vacuum level, it is not possible to obtain both the purity and recovery exceeding 90%. When the evacuation pressure is increased to P_L=0.05 bar, the performance of the cycle

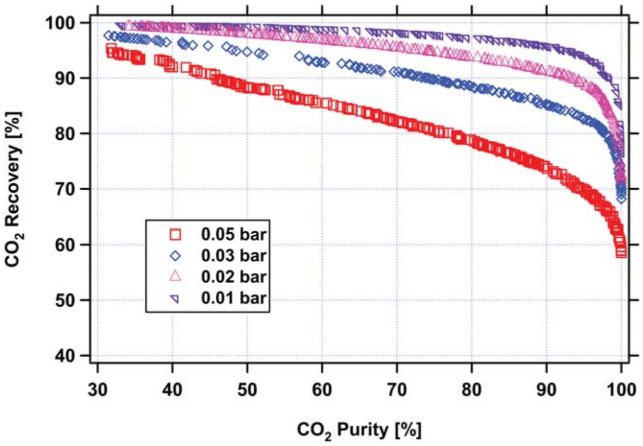

Figure 3. The effect of P_L on purity and recovery Pareto fronts for the basic 4-step VSA cycle.

The pressure values in the legend are the lower bounds of P_L. [Color figure can be viewed in the online issue, which is available at wileyonlinelibrary.com.]

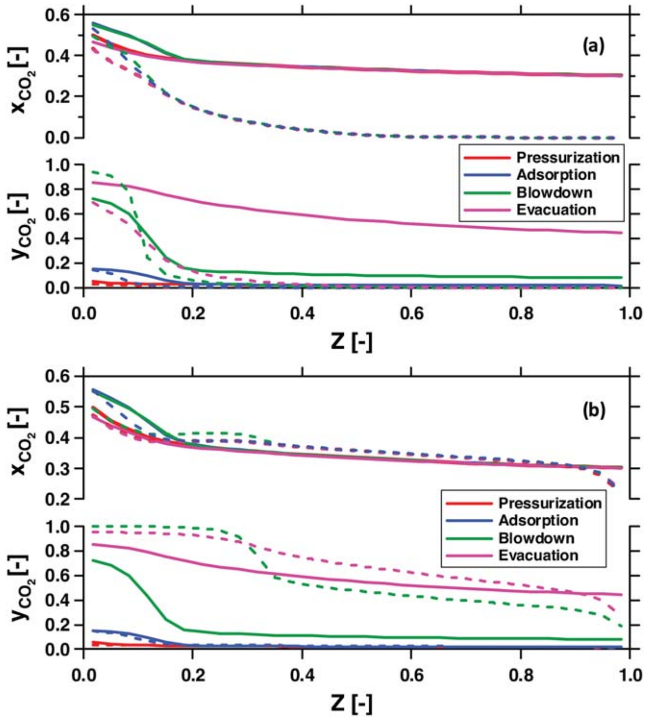

Figure 4. CO_2 gas and solid-phase column profiles.

Solid lines for the basic 4-step VSA cycle for the following conditions in both (a) and (b): $Pu = 80\%$ and $Re = 88\%$, $t_{press} = 20$ s, $t_{ads} = 74.6$ s, $t_{bd} = 60.1$ s, $t_{evac} = 85.4$ s, $P_I = 0.17$ bar, $P_L = 0.03$ bar, and $v_{feed} = 0.27$ m s^{-1}. The broken lines are for the 4-step VSA cycle with LPP for (a) $Pu = 80.2\%$ and $Re = 99.5\%$, $t_{ads} = 64.64$ s, $t_{bd} = 172.80$ s, $t_{evac} = 141.30$ s, $P_I = 0.07$ bar, $P_L = 0.03$ bar, and $v_{feed} = 0.23$ m s^{-1}; (b) $Pu = 97.4\%$ and $Re = 88.2\%$, $t_{ads} = 53.15$ s, $t_{bd} = 141.76$ s, $t_{evac} = 131.21$ s, $P_I = 0.05$ bar, $P_L = 0.03$ bar, and $v_{feed} = 0.33$ m s^{-1}. [Color figure can be viewed in the online issue, which is available at wileyonlinelibrary.com.]

drops drastically. In the previous study (see Ref 41), the possibility of increasing the feed pressure to boost process performance was explored, but it was concluded that this approach increased energy consumption. The alternative to pressurizing the feed is to consider more advanced cycles involving reflux and energy saving measures, which is the central theme of the current work.

To modify the 4-step cycle to attain the desired purity and recovery while keeping the vacuum pressure ≥ 0.03 bar, it is useful to study the axial CO_2 concentration profiles in the gas and solid phases of the column at the end of each step at CSS. To this end, let us consider an arbitrary point on the Pareto front for the lower bound of 0.03 bar on P_L, in Figure 3, yielding $Pu = 80\%$, $Re = 88\%$. This corresponds to the following operating conditions: $t_{press} = 20$ s, $t_{ads} = 74.6$ s, $t_{bd} = 60.1$ s, $t_{evac} = 85.4$ s, $P_I = 0.17$ bar, $P_L = 0.03$ bar, and $v_{feed} = 0.27$ m s^{-1}. The column profiles for gas (y_{CO_2}) and solid ($x_{CO_2} = q_{CO_2}/q_{sb,N_2}$) phase CO_2 concentrations are shown in Figure 4. From the gas-phase composition profile at the end of the adsorption and blowdown steps, it is clear from the long tails in the gas-phase profiles that CO_2 is lost in these steps which results in a loss of recovery. The loss of CO_2 is further evident from the profiles of CO_2 molar flow rate at the exit of the column during these two steps as shown in Figure 5. The presence of the tail in the CO_2 profile prevents the optimizer from choosing a blowdown pressure lower than 0.17 bar that could facilitate more nitrogen removal during the blowdown step. This could increase CO_2 purity in the extract product at the cost of recovery. Similarly, the optimizer chooses neither a higher feed velocity nor a longer feed duration for the adsorption step, which also could increase CO_2 purity at the expense of its recovery. Therefore, it would be desirable to reflux the effluent streams from the adsorption and blowdown steps to reduce the loss of CO_2 thereby increasing its recovery. The effluent from the adsorption step can be utilized either as LR and/or for LPP. The effluent from the blowdown step can also be used to partially repressurize one or more successive columns through PEs. Hence, additional cycle configurations shown in Figure 6 are generated, namely, 4-step cycle with LPP (Figure 6a), 5-step cycle with LPP and LR (Figure 6b), and 6-step cycle with both light and heavy reflux (Figure 6c). Further, the addition of PE yields three more configurations,

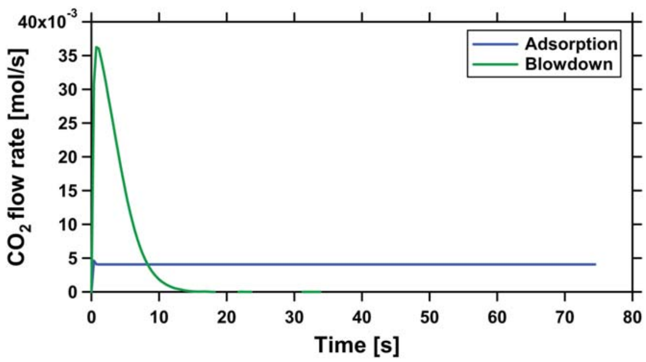

Figure 5. CO_2 loss during the adsorption and blowdown steps in the basic 4-step VSA cycle for the following conditions: $Pu = 80\%$ and $Re = 88\%$, $t_{press} = 20$ s, $t_{ads} = 74.6$ s, $t_{bd} = 60.1$ s, $t_{evac} = 85.4$ s, $P_I = 0.17$ bar, $P_L = 0.03$ bar, and $v_{feed} = 0.27$ m s^{-1}.

Losses during the adsorption and blowdown steps are 0.304 and 0.168 mol, respectively. [Color figure can be viewed in the online issue, which is available at wileyonlinelibrary.com.]

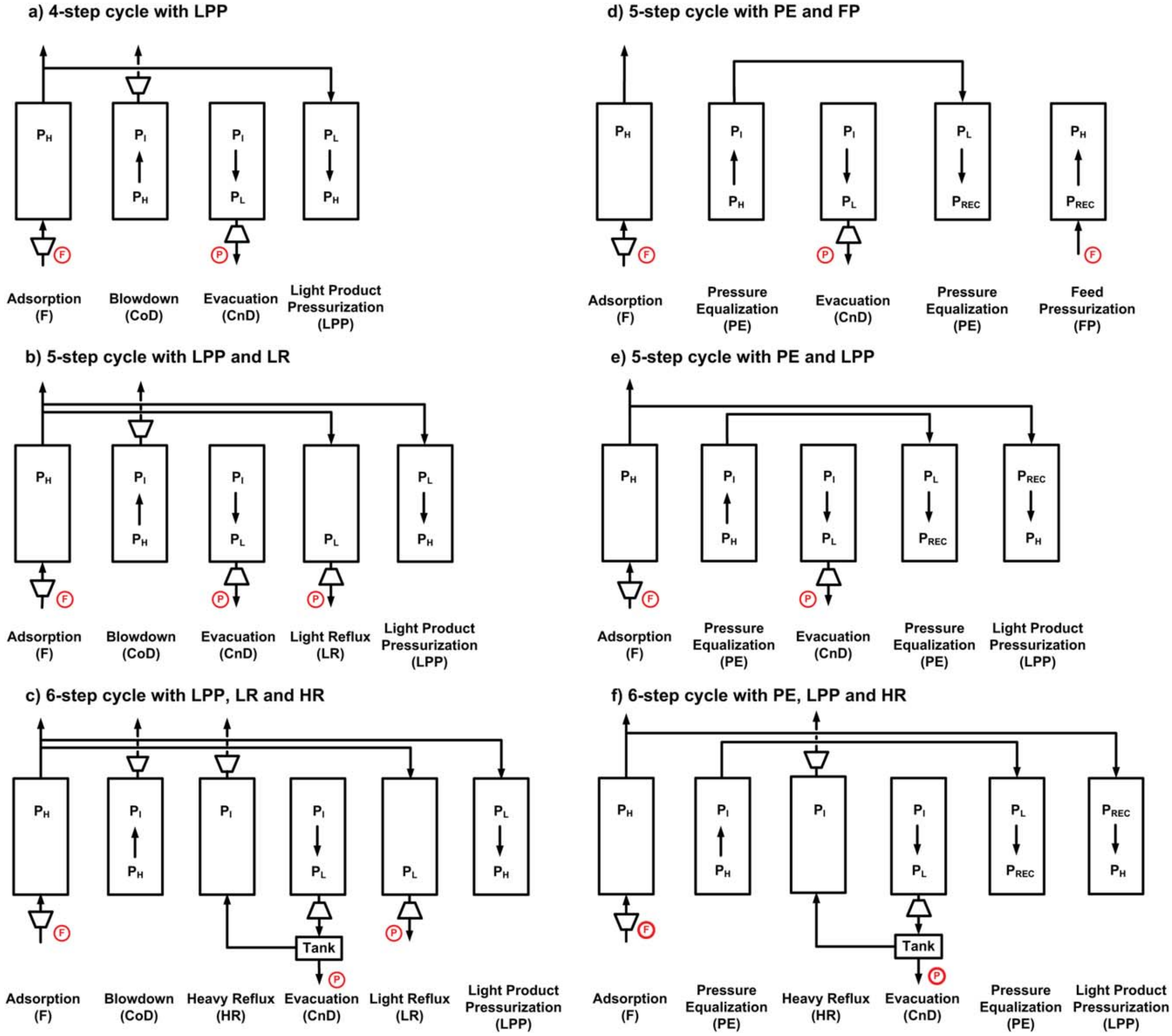

Figure 6. Schematics of various VSA cycles analyzed for postcombustion CO_2 capture.

The steps in which feed introduction and product removal occur are shown as F and P, respectively. [Color figure can be viewed in the online issue, which is available at wileyonlinelibrary.com.]

namely, 5-step cycle with PE and flue gas pressurization (Figure 6d), 5-step cycle with PE and LPP (Figure 6e), and 6-step cycle with PE, LPP, and HR (Figure 6f).

4-Step cycle with LPP

In this configuration, the feed pressurization step in the basic 4-step cycle is substituted with LPP. The effluent from the adsorption step is used to pressurize the column in the reverse direction, that is, from $z = L$. The time-dependent values of flow, composition, and temperature of the pressurization gas used during the LPP step come from the effluent of the previous adsorption step, which are stored in a data buffer. The duration of the LPP step is the time required for the column to reach P_H, and it depends on the flow rate of the effluent from the adsorption step. Thus, it cannot be fixed *a priori*. However, its maximum duration is set to be the duration of the adsorption step. In a multibed operation, a proper schedule can be worked out to implement LPP such that the effluent from the adsorption step is directly fed to the bed undergoing pressurization. Therefore, by implementing LPP in our one-bed simulation model using the data buffer, we are not compromising the actual physics of the operation or computational accuracy in any way. If the effluent stream is not sufficient to pressurize the column up to P_H, then the feed pressurization step, using the flue gas, is added to complete the pressurization. The same decision variables as the basic 4-step cycle are used in the optimization problem and their lower and upper bounds are shown in Table 3.

The Pareto front for this cycle is shown in Figure 7. Clearly, the LPP step has improved both purity and recovery compared to the basic 4-step cycle for evacuation pressures ≥ 0.03 bar. There are also many points on the Pareto front that give purity and recovery well above 90%. A careful observation of the optimal solution (not reported here) corresponding to the Pareto points reveals that the optimizer always chooses P_L near its lower bound. This trend is also observed for other cycles. To understand the beneficial effect of LPP on purity and recovery, we compare the column profiles of two Pareto points for the 4-step cycle with LPP and

Table 3. Decision Variables and Corresponding Lower and Upper Bounds Provided to the Optimizer for Each Cycle

Cycle	t_{ads} [s]	t_{bd}/t_{PE} [s]	t_{HR} [s]	θ [−]	t_{evac} [s]	t_{LR} [s]	P_I [bar]	P_L [bar]	v_{feed} [m s−1]
Basic 4-step	20–100	30–200	–	–	30–200	–	0.05–0.5	0.03–0.5	0.1–2
4-step with LPP	20–100	30–200	–	–	30–200	–	0.03–0.5	0.03–0.5	0.1–2
5-step with LPP and LR	20–100	30–200	–	–	30–200	1–15	0.03–0.5	0.03–0.5	0.1–2
6-step with LPP, LR, and HR	20–100	30–200	1–200	0.02–0.9	30–200	1–15	0.03–0.5	0.03–0.5	0.1–2
5-step with PE and FP	20–100	30–200	–	–	30–200	–	0.03–0.5	0.03–0.5	0.1–2
5-step with PE and LPP	20–100	30–200	–	–	30–200	–	0.03–0.5	0.03–0.5	0.1–2
6-step with PE, LPP, and HR	20–100	30–200	1–200	0.02–0.9	30–200	–	0.03–0.5	0.03–0.5	0.1–2

the basic 4-step cycle discussed earlier ($Pu = 80\%$ and $Re = 88\%$). For the first Pareto point (cf. Figure 4a), the CO_2 purity of the cycle with LPP is the same as that of the basic 4-step cycle, while the recovery is higher (99.5% compared to 88%). For the second point (cf. Figure 4b), the recovery is the same but the purity is higher (97.4% compared to 80%). One can clearly see from Figure 4a that by pressurizing the column in the reverse direction with the nitrogen-rich effluent stream from the adsorption step, the tails in the column profiles at the end of the adsorption and blowdown steps are diminished significantly, which lowers the CO_2 loss in these steps resulting in higher recovery from the evacuation step. Essentially, the consequence of adding the LPP step is to push the CO_2 front backward into the column. For the case shown in Figure 4b, the LPP step allows

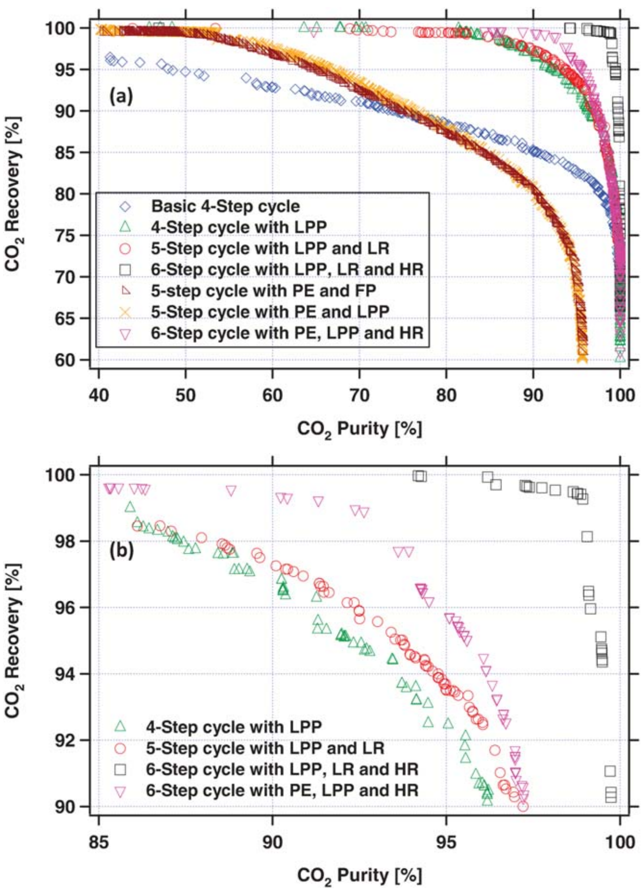

Figure 7. The purity-recovery Pareto fronts for the six VSA configurations explored in this study.

The Pareto fronts for the cycles that meet the 90% purity-recovery requirements are plotted on the magnified axes in (b) for clarity. [Color figure can be viewed in the online issue, which is available at wileyonlinelibrary.com.]

the optimizer to choose a lower P_I of 0.05 bar compared to the basic 4-step cycle. This helps remove more N_2 during the blowdown step, while retaining CO_2. Therefore, the purity of CO_2 is also higher.

5-Step cycle with LPP and LR

A common extension of LPP is LR, which is included in the cycle after the evacuation step with product collection taking place from the evacuation and LR steps (Figure 6b). In this cycle, a portion of the effluent stream from the adsorption step is first used as a LR, whereas the rest is used for LPP. Hence, the maximum duration of the LPP step is set to be ($t_{ads} - t_{LR}$). Similar to the previous cycle, if there is insufficient effluent gas from the adsorption step to complete pressurization, a feed pressurization step is incorporated. The time-dependent values of the flow, composition and temperature of the purge and pressurization gases used during the LR and LPP steps come from the effluent of the previous adsorption step stored in the data buffer. The main goal of the LR step is to desorb more CO_2 from the solid phase to increase the recovery. The bounds for the decision variables are listed in Table 3. The Pareto front for this cycle, shown in Figure 7, reveals a marginal improvement compared to the 4-step cycle with LPP. Key decision variables corresponding to the Pareto front are shown in Figure 8. It is seen that the optimal durations of the LR step are populated in the range of 1–3 s, that is, near the lower bound. This suggests that the LR step should be at best of short duration and choosing a longer duration contaminates the CO_2 product by allowing the N_2 front to reach the feed-end. Further, it is shown in Figure 8 that the optimal v_{feed} is below 1 m s^{-1}. Higher-feed velocity during adsorption step causes the CO_2 front to breakthrough which results in lower CO_2 recovery. In summary, addition of the LR step improves process performance marginally and its implementation must be carefully evaluated owing to short durations.

6-Step cycle with LPP, LR, and HR

From the analogy between adsorption and distillation, one way to improve the purity of the heavy component is to reflux the heavy product stream into the column. In this study, we have considered the 6-step cycle shown in Figure 6c, which includes both HR and LR steps. A fraction (θ) of the stream from the evacuation step is collected in a tank and refluxed into the column during the HR step. The main idea of adding the HR step is to enrich the feed end with CO_2 by displacing the lighter component prior to the evacuation step. In this study, we have sequenced the HR step after the blowdown step at a subatmospheric intermediate pressure. This is because performing the HR step before the blowdown step leads to a significant loss of CO_2 during the blowdown step. Furthermore, refluxing at the lower pressure

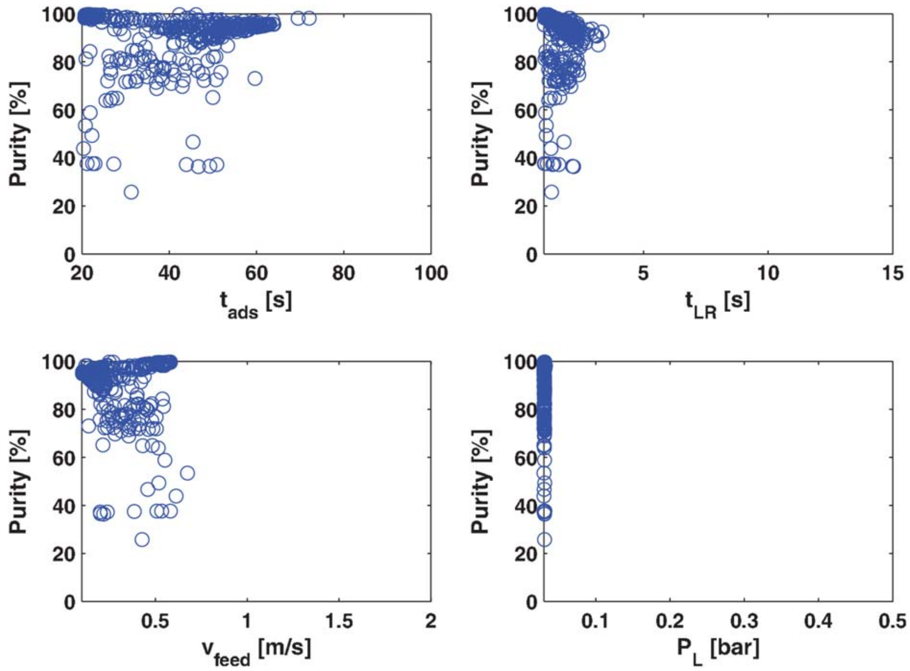

Figure 8. The decision variables corresponding to the Pareto front of the 5-step VSA cycle with LPP and LR shown in Figure 7.

[Color figure can be viewed in the online issue, which is available at wileyonlinelibrary.com.]

helps to reduce reflux ratio and hence the recovery loss. Note that the HR step requires an additional vacuum pump at the light-product end of the column to maintain the column pressure at the intermediate level. The reflux tank acts as the buffer necessary to maintain a constant feed rate of the reflux stream. The duration of this step, t_{HR}, and reflux ratio, θ, are also considered as decision variables and their lower and upper bounds are given in Table 3. In addition, we restrict t_{HR} to be less than the duration of the evacuation step. The inlet velocity to this step is calculated from the following mass-balance equation

$$v_{HR} = \frac{\theta \times \text{mole}_{\text{out}}|_{\text{evac}}}{t_{HR} A \varepsilon \frac{P|_{z=0}}{RT_{\text{feed}}}} \tag{8}$$

The Pareto front for the 6-step configuration with HR and LR is included in Figure 7. The HR step increases the CO_2 purity significantly and the Pareto front is pushed toward the top right corner. The optimal durations of the HR step vary between 5 and 8 s, whereas the optimal reflux ratio varies between 0.7 and 0.85. The column profiles at the end of each step for the operating conditions on the Pareto front with $Pu = 98.5\%$ and $Re = 99.4\%$ are shown in Figure 9. As we can see from this figure, the tail of the CO_2 profile at the end of the HR step is almost at $z = L$, hence controlling the CO_2 front during the HR step is critical. Any longer HR step would result in the breakthrough of CO_2 at the light-product end and reduce the recovery.

Cycles with one PE step

Substituting the blowdown step in the basic 4-step cycle with a forward PE step gives us a 5-step cycle with PE. In this cycle, the duration of the feed pressurization step is fixed at 20 s. During the PE step, the end at $z = L$ of the high-pressure column (donor) is connected to the same end of the low-pressure column (receiver). The effect of this step on the donor column is similar to the forward blowdown step except that a vacuum pump is not needed, thereby providing an opportunity to reduce fixed cost and energy consumption. However, the intermediate pressure can no longer be a decision variable, unlike in the blowdown step, which uses a vacuum pump and a feedback pressure controller. Hence, in contrast to the blowdown step, here CO_2 is conserved but N_2 removal from the donor bed is also limited by the final pressure achieved after each PE. In this study, the PE step has been implemented using single column simulation. In this approach, the intermediate pressure (P_I) has to be chosen in a way that the amount of the gas that comes out of the column is sufficient to pressurize the receiver column from P_L to P_I. In other words, in the PE step, the final

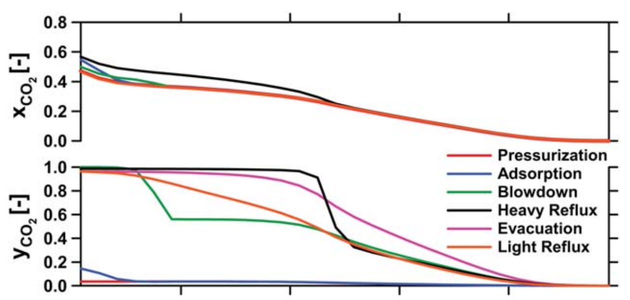

Figure 9. CO_2 gas and solid-phase column profiles for the 6-step VSA cycle with LPP, LR, and HR for the following conditions: $Pu = 98.5\%$ and $Re = 99.4\%$, $t_{ads} = 59.22$ s, $t_{bd} = 35.19$ s, $t_{HR} = 5.07$ s, $t_{evac} = 104.61$ s, $t_{LR} = 1.34$ s, $P_I = 0.054$ bar, $P_L = 0.03$ bar, $\theta = 0.82$, and $v_{feed} = 0.2$ m s^{-1}.

[Color figure can be viewed in the online issue, which is available at wileyonlinelibrary.com.]

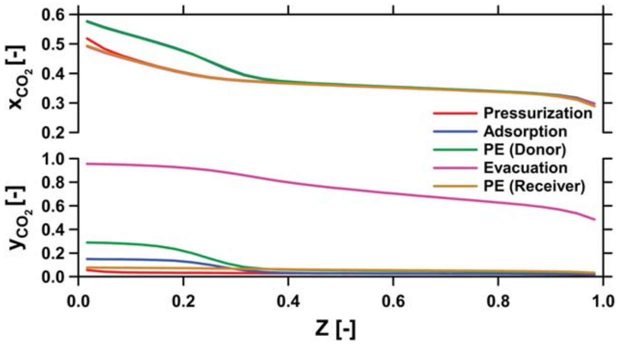

Figure 10. CO_2 gas and solid-phase column profiles for the 5-step VSA cycle with PE and FP for the following conditions: $Pu = 74.65\%$ and $Re = 90.18\%$, $t_{press} = 20.0$ s, $t_{ads} = 83.59$ s, $t_{PE} = 60.0$ s, $t_{evac} = 130.0$ s, $P_L = 0.03$ bar, and $v_{feed} = 0.56$ m s^{-1}.

[Color figure can be viewed in the online issue, which is available at wileyonlinelibrary.com.]

pressures of the two column involved must be the same and the loss and gain of mass between the columns should be the same. Therefore, the single column analogue of simulating PE step should ideally be solved by trial and error which is computationally time consuming, particularly in the context of optimization. Hence, the intermediate pressure is not decision variable in the optimization problem. However, to eliminate the need for trial and error, we have approximated the intermediate pressure using the following equation

$$P_I \sim \frac{P_H + P_L}{2} - \kappa \tag{9}$$

The value of κ is estimated to be 0.041 bar through a number of simulations. Using this value, it is also observed that the pressure of the receiver column at the end of PE is always lower than that of the donor column, thereby satisfying the physics of the operation. Although, this approach may not replicate exactly the PE step in a multicolumn simulation, the small deviation is expected to have negligible impact on the final results. The ranges for the decision variables in the 5-step cycle with PE are given in Table 3. The Pareto front for this cycle is compared in Figure 7 with those from the other cycles discussed so far. The difference between P_{REC} and P_I for the Pareto points varies in the range 0.01–0.1 bar. This Pareto front shows significantly lower purity compared to the cycles with the blowdown step and this cycle is unable to give the desired purity-recovery ($\geq 90\%$) for carbon capture. Due to the high-intermediate pressure in cycles with PE, less N_2 is removed from the donor column. Thus, more N_2 comes out with CO_2 during the evacuation step, which reduces CO_2 purity significantly. This argument is well supported by the column profiles shown in Figure 10 for a point on the Pareto curve corresponding to a recovery of 90.18% and purity of 74.65%. It is clearly seen in the figure that considerably more nitrogen is present in the donor bed at the end of PE which results in lower CO_2 purity. Further, replacing the flue gas pressurization by the LPP step in this cycle gives us a 5-step cycle with PE and LPP. However, the Pareto front for this cycle is nearly indistinguishable from the one for the 5-step cycle with PE. Recall that cycles with LPP allowed lower pressure in the blowdown step without losing CO_2, which improved its purity and recovery. Clearly, with PE, the advantage of LPP cannot be fully exploited. Hence, LPP with PE is not as beneficial as LPP with blowdown.

We have discussed the beneficial effect of the HR step earlier to improve CO_2 purity. Therefore, we also explored the option of adding the HR step to the 5-step cycle with PE and LPP, which becomes a 6-step cycle with PE, LPP, and HR as shown schematically in Figure 6f. The Pareto front for this 6-step cycle, as shown in Figure 7, improves on that for the 5-step cycle with PE and LPP by refluxing 65–90% of the evacuation stream. Another alternative to improve the Pareto front of the 5-step cycle with PE to approach 90% purity and recovery without using the HR step is to perform more PE steps. Although this will reduce the energy consumption compared to the cycle with forward blowdown, adding more steps will, however, lower the productivity due to a longer cycle time.

Minimization of Energy Consumption and Maximization of Productivity

In the previous section, we have analyzed six VSA configurations in terms of their purity-recovery Pareto fronts. However, these Pareto fronts do not provide any information about the energy required to capture CO_2, known as parasitic energy in the power industry. They also do not provide any idea of plant productivity. It is very important from the economical point of view that the capture energy is minimized while maximizing the productivity. Unlike steady state separation processes, cyclic operations offer a trade-off between energy consumption and productivity. In this section, this issue is addressed by optimizing the operating conditions of the VSA processes to minimize the energy consumption and maximize the productivity while ensuring 90% purity and recovery. Specifically, the optimization problem is cast as

$$\begin{aligned} \mathrm{Min}\, J_1 &= \psi_1 E + \lambda_1 \left[\max\left(0, Pu_{\mathrm{target}} \text{-} Pu_{\mathrm{CO2}}\right)\right]^2 \\ &\quad + \lambda_2 \left[\max\left(0, Re_{\mathrm{target}} \text{-} Re_{\mathrm{CO2}}\right)\right]^2 \\ \mathrm{Min}\, J_2 &= \frac{\psi_2}{Pr} + \lambda_1 \left[\max\left(0, Pu_{\mathrm{target}} \text{-} Pu_{\mathrm{CO2}}\right)\right]^2 \\ &\quad + \lambda_2 \left[\max\left(0, Re_{\mathrm{target}} \text{-} Re_{\mathrm{CO2}}\right)\right]^2 \end{aligned} \tag{10}$$

where ψ_i and λ_i are penalty functions; Pu_{target}, Re_{target} are the target purity and recovery values, respectively.

Obviously, only the cycles that can provide purity and recovery higher than 90% are considered. Thus, only the following four cycles qualify for further analysis: 4-step with LPP, 5-step with LPP and LR, 6-step with LPP, LR and HR, and 6-step with PE, LPP, and HR. The bounds on the decision variables used earlier and given in Table 3 are kept unchanged. The obtained results are shown in Figure 11. As expected, there is a trade-off between energy consumption and productivity, which is indicated by the Pareto fronts in Figure 11. As the operating conditions corresponding to every point on the Pareto curve meet the requirements of 90% purity and recovery, one can now choose the desired energy-productivity performance from the Pareto front and trace back the operating conditions corresponding to that point.

In the discussion so far in this section, P_L is ≥ 0.03 bar. To explore any potential advantage of allowing lower P_L, we repeat the energy-productivity Pareto curve for the 4-step

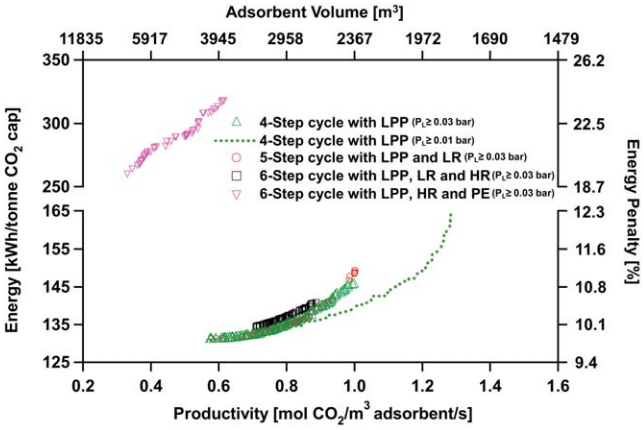

Figure 11. Energy-productivity Pareto fronts for the four VSA cycles of different configurations that meet 90% purity-recovery constraints.

The Pareto fronts for the 4-step cycle with LPP for $P_L \geq 0.01$ bar and $P_L \geq 0.03$ bar are identical in the initial part. The extension $(\cdots)$ is a result of lowering the P_L from 0.03 to 0.01 bar. [Color figure can be viewed in the online issue, which is available at wileyonlinelibrary.com.]

cycle with LPP for $P_L \geq 0.01$ bar, as shown in Figure 11. Expectedly, the initial part of the Pareto front is identical with the earlier one. However, it extends the productivity window from ≈1.0 to 1.3 mol CO_2/m^3 adsorbent/s. Such deep vacuum levels are known to be challenging in practice for large scale processes. However, given the enormity of the plant size for carbon capture, the resulting significant increase in productivity (albeit at the expense of slight increase in energy penalty) makes the challenge of attaining deeper vacuum a worthwhile undertaking.

The Pareto front of the 5-step cycle with LPP and LR, and 6-step cycle with LPP, LR, and HR are quite close to that of the 4-step cycle with LPP. This can be explained by studying the optimal decision variables for the various Pareto points of the 6-step cycle with LPP, LR, and HR shown in Figure 12. It is clear from this figure that the optimizer prefers the minimum possible durations, that is, 1 s, for LR, and also the minimum durations and reflux ratios for HR. In order words, the optimizer is trying to reduce this 6-step cycle to the 4-step cycle with LPP to maximize productivity and minimize energy consumption. The slight difference between the Pareto curves for the two aforementioned cycles results from the imposed artificial lower bounds of t_{LR}, t_{HR}, and θ (1 s, 1 s, and 0.02), which prevent the optimizer to completely eliminate these steps. This is merely to avoid simulating a step with unrealistically small duration. Recall that adding the HR step to the 4-step cycle with LPP improves the performance in terms of purity and recovery. However, this increases the energy consumption, because the column needs to be maintained at subatmospheric pressure during the HR step. As with any reflux, HR increases the amount of the gas collected from the evacuation step, which also increases energy consumption. Furthermore, as discussed earlier, t_{LR} is hitting the lower bound as longer duration causes the contamination of the feed end with N_2, thus, decreasing CO_2 purity. Last, it should be noted that additional vacuum pumps are required to execute the HR and LR steps.

The energy-productivity optimization is also carried out for the 6-step cycle with PE and HR. As may be seen in Figure 11, the energy consumption for this cycle is significantly higher than that for the 4-step cycle with LPP and the productivity is also lower. The need for the blowdown vacuum pump is eliminated because the blowdown step is replaced

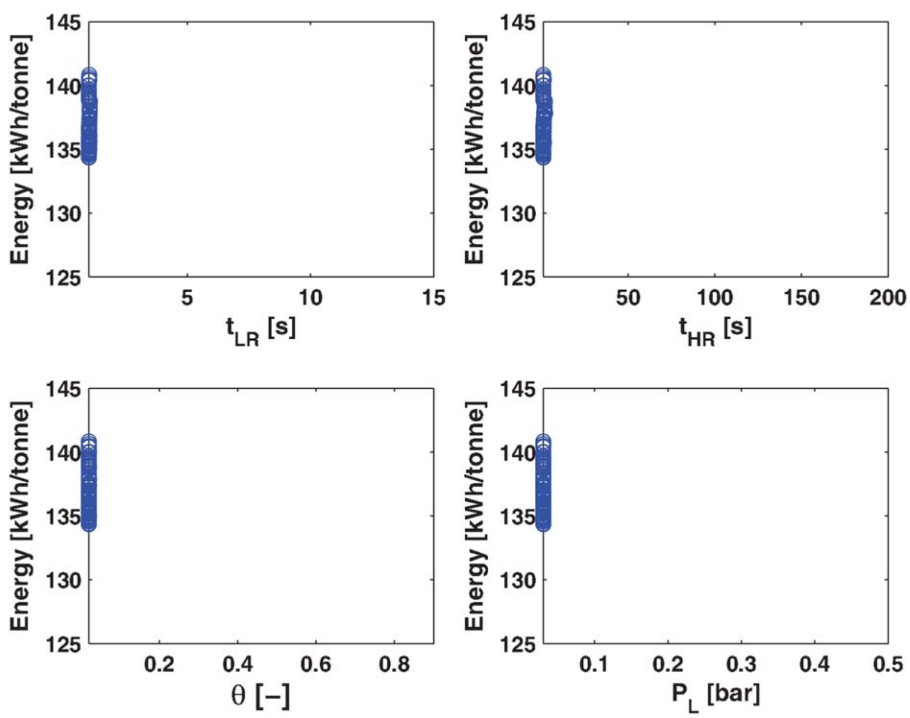

Figure 12. The decision variables corresponding to the Pareto front of the 6-step VSA cycle with PE, LPP, and HR shown in Figure 11.

[Color figure can be viewed in the online issue, which is available at wileyonlinelibrary.com.]

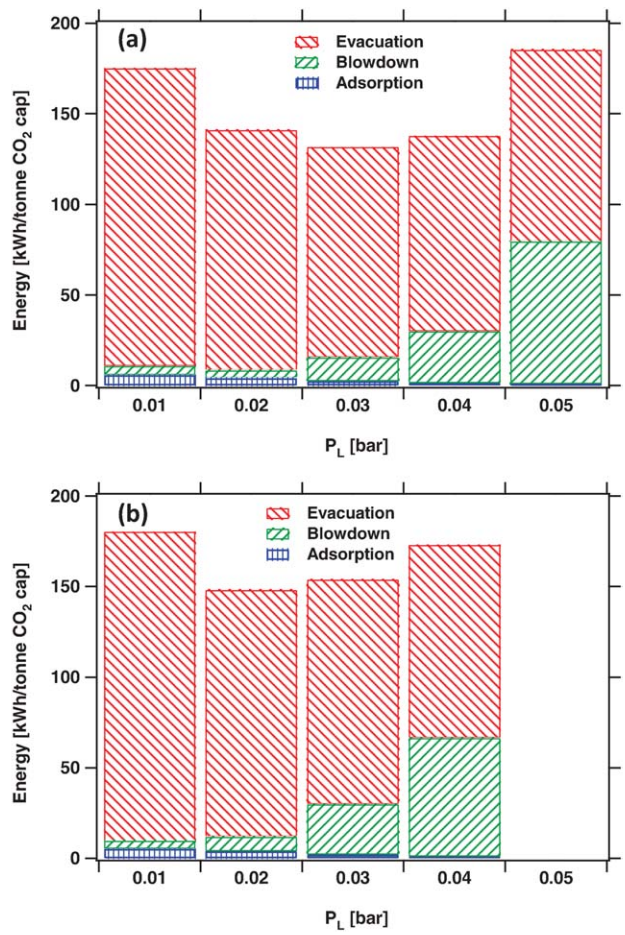

Figure 13. (a) Minimum energy for the 4-step VSA cycle with LPP at different evacuation pressures with 90% purity.

(b) Minimum energy for the 4-step VSA cycle with LPP at different evacuation pressures with 95% purity. [Color figure can be viewed in the online issue, which is available at wileyonlinelibrary.com.]

by the PE step. However, as the desired purity and recovery are not attained without high-reflux ratio in the HR step, the energy consumption in both HR and evacuation steps increase the overall energy requirement significantly. Moreover, the high-reflux ratio also reduces the productivity. It may be argued that a series of PE steps in principle may help improve the purity-recovery Pareto front of the 5-step cycle with PE and LPP to approach that of the 4-step cycle with LPP. However, it is also easy to conclude from Figure 7 that this would require several PE steps, and hence the option of using PE in place of blowdown needs to be evaluated carefully. According to Figure 11, the minimum energy penalty for the 4-step VSA cycle with LPP is 131 kWh/tonne CO_2 captured (10% energy penalty) at the following operating conditions, $t_{ads} = 99.86$ s, $t_{bd} = 30.53$ s, $t_{evac} = 116.82$ s, $P_I = 0.16$ bar, $P_L = 0.03$ bar, and $v_{feed} = 0.46$ m s^{-1}, out of which the contribution of the forward blowdown step is only 13.2 kWh/tonne CO_2 captured (~10% of the total energy penalty). Hence, if it is indeed possible to meet the 90% purity-recovery requirements by a series of PE steps, then it would at best reduce the energy penalty to ~9%. However, the drastic drop in productivity due to multiple PE steps will far outweigh this marginal reduction in energy penalty.

It is also interesting to study the effect of evacuation pressure on the energy consumption of the 4-step cycle with LPP. To this end, we minimize the energy consumption of this cycle with evacuation pressures fixed at 0.01, 0.02, 0.03, 0.04, and 0.05 bar. For the 4-step VSA cycle with LPP, 0.05 bar is the upper limit of the evacuation pressure that is able to meet the 90% purity-recovery constraints. The minimum energy consumptions for these pressures are shown in Figure 13a. Interestingly, $P_L = 0.03$ bar gives the minimum energy consumption. Furthermore, the energy required for the blowdown step increases with evacuation pressure. This can be explained by the decrease in the blowdown pressure (Table 4) required to satisfy the desired purity-recovery levels.

It is clear from the above discussion that the 4-step VSA cycle with LPP offers the minimum energy consumption for 90% purity and recovery. To evaluate the potential of the 4-step VSA cycle with LPP for higher purities, the optimization procedure was repeated with constraints of $Pu \geq 95\%$ and $Pu \geq 97\%$ while maintaining the constraint of $Re \geq 90\%$. The Pareto fronts for this study are shown in Figure 14. Both minimum energy consumption and the corresponding productivity values worsen with increased purity requirement. In all optimal solutions, P_L invariably converged to its lower bound of 0.03 bar. Therefore, we repeated the analysis presented in Figure 13a now for $Pu \geq 95\%$. The results shown in Figure 13b indicate that the minimum energy consumption now occurs at $P_L = 0.02$ bar, although the difference between operating the unit at low pressures of 0.02 and 0.03 bar is at best marginal. By comparing the conditions for 95% CO_2 purity with those for 90% CO_2 purity in Table 4, it is clear that the energy increase for a particular value of P_L is mainly from the blowdown step as more N_2 needs to be removed.

Table 4. Operating Conditions Corresponding to the Minimum Energy for the 4-step VSA Cycle with LPP at Different Evacuation Pressures

Purity [%]	P_L [bar]	t_{ads} [s]	t_{bd} [s]	t_{evac} [s]	P_I [bar]	v_{feed} [m s^{-1}]	Total Energy [kWh tonne^{-1}]
90	0.01	67.80	37.14	95.32	0.26	1.18	175.16
	0.02	99.98	45.20	192.63	0.28	0.83	140.90
	0.03	99.86	30.53	116.82	0.16	0.46	131.04
	0.04	99.33	60.55	80.50	0.11	0.27	137.73
	0.05	75.37	74.21	157.87	0.08	0.18	185.34
95	0.01	99.58	103.30	196.52	0.20	1.09	180.13
	0.02	99.14	32.09	195.09	0.14	0.80	147.94
	0.03	84.79	34.36	148.56	0.08	0.41	153.80
	0.04	66.74	66.45	181.43	0.06	0.23	172.91

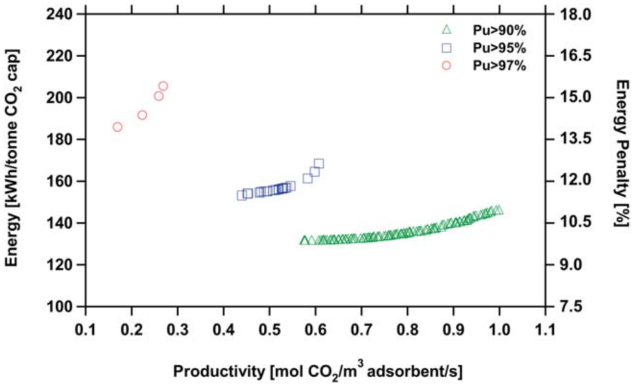

Figure 14. Effect of CO_2 purity on energy-productivity Pareto fronts for the 4-step VSA process.

All three purity requirements are subject to a 90% recovery constraint and $P_L \geq 0.03$ bar. [Color figure can be viewed in the online issue, which is available at wileyonlinelibrary.com.]

Conclusions

In this work, we have systematically developed and evaluated six promising VSA configurations for postcombustion CO_2 capture from dry flue gas using Zeochem zeolite 13X as the adsorbent. A GA-based multiobjective optimization algorithm has been used to generate full purity-recovery Pareto fronts to evaluate these cycles. Unlike single objective optimization, this algorithm offers a set of optimal operating conditions, thereby allowing the process engineer more freedom in balancing conflicting objectives. Our full scale optimization was made possible by an efficient implementation of the rigorous process simulation model based on the weighted essentially non-oscillatory (WENO) finite volume technique. This study provides physical insights on the roles of LPP, LR, HR, and PE in the context of an extract cycle and leads to the following important conclusions:

1. A simple 4-step VSA cycle with LPP is able to achieve 90% purity-recovery requirements with a minimum energy consumption of 131 kWh/tonne CO_2 captured at a productivity of 0.57 mol CO_2/m^3 adsorbent/s. This requires an evacuation pressure of 0.03 bar. This energy consumption increases to 154 kWh/tonne CO_2 captured at a productivity of 0.44 mol CO_2/m^3 for 95% CO_2 purity. The 4-step cycle with LPP is much simpler than some of the more complex VSA cycles reported in the literature with comparable energy performance.
2. The energy-productivity Pareto curve for the 4-step cycle with LPP is nearly flat such that a small (~1%) increase in energy penalty increases the productivity by 70%. The productivity window can be extended significantly by further lowering P_L.
3. In the basic 4-step VSA process studied earlier,[41] the minimum energy for attaining 90% purity-recovery requirements was 149 kWh/tonne CO_2 captured and the evacuation pressure was 0.02 bar. Beyond this evacuation pressure, feed pressurization was required to achieve 90% purity-recovery, adding substantially to energy penalty. In contrast, the use of LPP to replace feed pressurization not only reduces the energy consumption at all acceptable evacuation pressures but also extends the operable VSA range of evacuation pressure to 0.05 bar. This widens the window for industrial implementation of low-energy operation without resorting to expensive feed pressurization.
4. In addition to the 4-step cycle with LPP, 5-step cycle with LPP and LR, 6-step cycle with LPP, LR, and HR, and 6-step cycle with PE, LPP, and HR are also able to enrich CO_2 to 90% purity with 90% recovery. The best performing cycle based on purity and recovery is the 6-step cycle with LPP, LR, and HR. The CO_2 purity and recovery for this cycle are as high as $Pu = 98.5\%$ and $Re = 99.4\%$, respectively. However, the HR step is energetically unfavorable and thus, not preferred by the optimizer when minimizing energy consumption is the priority.

Acknowledgments

The work was carried out under the thematic strategic research program on carbon capture and utilization funded by A*STAR, Singapore. The authors acknowledge the contribution of Srinath Sridharan, National University of Singapore. We thank Zeochem for in-kind contribution of the adsorbent.

Notation

A = cross-sectional area of the column, m^2
b_0 = parameter in dual site Langmuir isotherm, m^3 mol^{-1}
C_{pa} = specific heat capacity of the adsorbed phase, J mol^{-1} K^{-1}
C_{pg} = specific heat capacity of the gas phase, J mol^{-1} K^{-1}
C_{ps} = specific heat capacity of the adsorbent, J kg^{-1} K^{-1}
C_{pw} = specific heat capacity of the column wall, J kg^{-1} K−1
d_0 = parameter in dual site Langmuir isotherm, m^3 mol^{-1}
D_m = molecular diffusivity, m^2 s^{-1}
h_{in} = inside heat-transfer coefficient, J m^{-2} K^{-1} s^{-1}
h_{out} = outside heat-transfer coefficient, J m^{-2}K^{-1} s^{-1}
K_w = thermal conductivity of column wall, J m^{-1} K^{-1} s^{-1}
K_z = effective gas thermal conductivity, J m^{-1} K^{-1} s^{-1}
L = column length, m
n_{comp} = number of components
P = pressure, Pa
P_{REC} = final pressure of pressure equalization step for the pressurized column, bar
q = concentration in the solid phase, mmol g^{-1}
q_{sb} = saturation concentration in the solid phase for site 1, mmol g^{-1}
q_{sd} = saturation concentration in the solid phase for site 2, mmol g^{-1}
r_{in} = column inner radius, m
r_{out} = column outer radius, m
r_p = particle radius, m
R = universal gas constant, Pa m^3 mol^{-1} K^{-1}
t = time, s
T = temperature, K
T_{feed} = feed temperature, K
T_a = ambient temperature, K
T_w = column wall temperature, K
U = internal energy, J mol^{-1}
v = interstitial velocity, m s^{-1}
x = dimensionless concentration in solid phase
y = composition in the gas phase
z = axial coordinate, m.

Greek letters

ε = bed voidage
ε_p = particle voidage
η = compression/evacuation efficiency
γ = adiabatic constant
μ = fluid viscosity, kg m^{-1} s^{-1}
ρ_s = adsorbent density, kg m^{-3}
ρ_w = wall density, kg m^{-3}
θ = reflux ratio
τ' = tortuosity.

Subscripts

ads = adsorption step
bd = blowdown step
evac = evacuation step
f = flue gas
feed = feed condition
H = high
HR = heavy reflux step
I = intermediate
L = low
LPP = light product pressurization
LR = light reflux step
out = stream coming out
press = pressurization step
PE = pressure equalization step
REC = receiver

Literature Cited

1. Intergovernmental Panel on Climate Change (IPCC). Special report on carbon dioxide capture and storage, Technical report. New York, NY: Cambridge University Press, 2005.
2. Katzer J. The future of coal, Technical report. Cambridge, MA: Massachusetts Institute of Technology, 2007.
3. Ebner A, Ritter J. State-of-the-art adsorption and membrane separation processes for carbon dioxide production from carbon dioxide emitting industries. *Sep Sci Technol.* 2009;44(6):1273–1421.
4. Aaron D, Tsouris C. Separation of CO_2 from flue gas: a review. *Sep Sci Technol.* 2005;40(1):321–348.
5. Xiao P, Zhang J, Webley P, Li G, Singh R, Todd R. Capture of CO_2 from flue gas streams with zeolite 13X by vacuum-pressure swing adsorption. *Adsorption.* 2008;14(4–5):575–582.
6. Agarwal A, Biegler LT, Zitney SE. A superstructure-based optimal synthesis of PSA cycles for post-combustion CO_2 capture. *AIChE J.* 2010;56(7):1813–1828.
7. Ruthven D, Farooq S, Knaebel K. Pressure Swing Adsorption. New York, NY: VCH Publishers, 1994.
8. Matz M, Knaebel K. Recycled thermal swing adsorption: applied to separation of binary and ternary mixtures. *Ind Eng Chem Res.* 1991; 30(5):1046–1054.
9. Merkel T, Zhou M, Baker R. Carbon dioxide capture with membranes at an IGCC power plant. *J Membr Sci.* 2012;389(0):441–450.
10. National Energy Technology Laboratory. Quality guidelines for energy system studies: CO_2 impurity design parameters, Technical report. National Energy Technology Laboratory, DOE/NETL-341/011212, 2012.
11. Reynolds S, Ebner A, Ritter J. Stripping PSA cycles for CO_2 recovery from flue gas at high temperature using a Hydrotalcite-like adsorbent. *Ind Eng Chem Res.* 2006;45(12):4278–4294.
12. Reynolds S, Mehrotra A, Ebner A, Ritter J. Heavy reflux PSA cycles for CO_2 recovery from flue gas: part I. Performance evaluation. *Adsorption.* 2008;14(2–3):399–413.
13. Zhang J, Webley P. Cycle development and design for CO_2 capture from flue gas by vacuum swing adsorption. *Environ Sci Technol.* 2008;42(2):563–569.
14. Zhang J, Webley P, Xiao P. Effect of process parameters on power requirements of vacuum swing adsorption technology for CO_2 capture from flue gas. *Energy Convers Manag.* 2008;49(2):346–356.
15. Li G, Xiao P, Webley P, Zhang J, Singh R, Marshall M. Capture of CO_2 from high humidity flue gas by vacuum swing adsorption with zeolite 13X. *Adsorption.* 2008;14(2–3):415–422.
16. Ko D, Siriwardane R, Biegler L. Optimization of pressure swing adsorption and fractionated vacuum pressure swing adsorption processes for CO_2 capture. *Ind Eng Chem Res.* 2005;44(21):8084–8094.
17. Chue K, Kim J, Yoo Y, Cho S, Yang R. Comparison of activated carbon and Zeolite 13X for CO_2 recovery from flue gas by pressure swing adsorption. *Ind Eng Chem Res.* 1995;34(2):591–598.
18. Park JH, Beum HT, Kim JN, Cho SH. Numerical analysis on the power consumption of the PSA process for recovering CO_2 from flue gas. *Ind Eng Chem Res.* 2002;41(16):4122–4131.
19. Choi WK, Kwon TI, Yeo YK, Lee H, Song H, Na BK. Optimal operation of the pressure swing adsorption (PSA) process for CO_2 recovery. *Korean J Chem Eng.* 2003;20(4):617–623.
20. Chou CT, Chen CY. Carbon dioxide recovery by vacuum swing adsorption. *Sep Purif Technol.* 2004;39(1–2):51–65.
21. Takamura Y, Narita S, Aoki J, Hironaka S, Uchida S. Evaluation of dual-bed pressure swing adsorption for CO_2 recovery from boiler exhaust gas. *Sep Purif Technol.* 2001;24(3):519–528.
22. Kikkinides E, Yang R, Cho S. Concentration and recovery of carbon dioxide from flue gas by pressure swing adsorption. *Ind Eng Chem Res.* 1993;32(11):2714–2720.
23. Na BK, Koo KK, Eum HM, Lee H, Song H. CO_2 recovery from flue gas by PSA process using activated carbon. *Korean J Chem Eng.* 2001;18(2):220–227.
24. Na BK, Lee H, Koo KK, Song H. Effect of rinse and recycle methods on the pressure swing adsorption process to recover CO_2 from power plant flue gas using activated carbon. *Ind Eng Chem Res.* 2002;41(22):5498–5503.
25. Shen C, Yu J, Li P, Grande C, Rodrigues A. Capture of CO_2 from flue gas by vacuum pressure swing adsorption using activated carbon beads. *Adsorption.* 2011;17(1):179–188.
26. Kapoor A, Krishnamurthy K, Shirley A. Kinetic separation of carbon dioxide from hydrocarbons using carbon molecular sieve. *Gas Sep Purif.* 1993;7(4):259–263.
27. Liu Z, Grande C, Li P, Yu J, Rodrigues A. Multi-bed vacuum pressure swing adsorption for carbon dioxide capture from flue gas. *Sep Purif Technol.* 2011;81(3):307–317.
28. Sircar S. Pressure swing adsorption. *Ind Eng Chem Res.* 2002;41(6): 1389–1392.
29. Vetukuri S, Biegler L, Walther A. An inexact trust-region algorithm for the optimization of periodic adsorption processes. *Ind Eng Chem Res.* 2010;49(23):12004–12013.
30. Nikolic D, Kikkinides E, Georgiadis M. Optimization of multibed pressure swing adsorption processes. *Ind Eng Chem Res.* 2009; 48(11):5388–5398.
31. Jiang L, Biegler LT, Fox VG. Simulation and optimization of pressure-swing adsorption systems for air separation. *AIChE J.* 2003; 49(5):1140–1157.
32. Cruz P, Santos J, Magalhes F, Mendes A. Cyclic adsorption separation processes: analysis strategy and optimization procedure. *Chem Eng Sci.* 2003;58(14):3143–3158.
33. Cruz P, Magalhes F, Mendes A. On the optimization of cyclic adsorption separation processes. *AIChE J.* 2005;51(5):1377–1395.
34. Biegler LT, Jiang L, Fox VG. Recent advances in simulation and optimal design of pressure swing adsorption systems. *Sep Purif Rev.* 2005;33(1):1–39.
35. Ko D, Siriwardane R, Biegler L. Optimization of a pressure-swing adsorption process using zeolite 13X for CO_2 sequestration. *Ind Eng Chem Res.* 2003;42(2):339–348.
36. Sankararao B, Gupta S. Multi-objective optimization of pressure swing adsorbers for air separation. *Ind Eng Chem Res.* 2007;46(11): 3751–3765.
37. Fiandaca G, Fraga E, Brandani S. A multi-objective genetic algorithm for the design of pressure swing adsorption. *Eng Optimiz.* 2009;41(9):833–854.
38. Bhaskar V, Gupta S, Ray A. Applications of multiobjective optimization in chemical engineering. *Rev Chem Eng.* 2000;16(1):1–54.
39. Rangaiah G. Multi-Objective Optimization: Techniques and Applications in Chemical Engineering, Vol. 1 in the Advances in Process Systems Engineering. Singapore: World Scientific, 2009.
40. Amanullah M, Mazzotti M. Optimization of a hybrid chromatography-crystallization process for the separation of Tröger's base enantiomers. *J Chromatogr A.* 2006;1107(1–2):36–45.
41. Haghpanah R, Majumder A, Nilam R, Rajendran A, Farooq S, Karimi IA, Amanullah M. Multi-objective optimization of a 4-step adsorption process for postcombustion CO_2 capture using finite volume technique. *Ind Eng Chem Res.* 2013;52(11):4249–4265.
42. Krishnamurthy S, Haghpanah R, Rajendran A, Farooq S. Adsorption and diffusion of CO_2 and nitrogen on 13X and silica gel. In: 14th Asia Pacific Confederation of Chemical Engineering (APCChE 2012), Singapore, 2012.
43. Deb K, Pratap A, Agarwal S, Meyarivan T. A fast and elitist multiobjective genetic algorithm: NSGA-II. *IEEE Trans Evol Comput.* 2002;6(2):182–197.

Manuscript received Jan. 18, 2013, revision received Apr. 24, 2013, and final revision received July 5, 2013.